Transient localized wave patterns and their application to migraine

Markus A. Dahlem[1, 2, a)] and Thomas M. Isele[2]
[1)] *Institute for Physics, Humboldt Universität zu Berlin, Berlin, Germany*
[2)] *Institute for Theoretical Physics, Technische Universität Berlin, Berlin, Germany*

(Dated: 6 November 2012)

Transient dynamics is pervasive in the human brain and poses challenging problems both in mathematical tractability and clinical observability. We investigate statistical properties of transient cortical wave patterns with characteristic forms (shape, size, duration) in a canonical reaction-diffusion model with mean field inhibition. The patterns are formed by a ghost near a saddle-node bifurcation in which a stable traveling wave (node) collides with its critical nucleation mass (saddle). Similar patterns have been observed with fMRI in migraine. Our results support the controversial idea that waves of cortical spreading depression (SD) have a causal relationship with the headache phase in migraine and therefore occur not only in migraine with aura (MA) but also in migraine without aura (MO), i. e., in the two major migraine subforms. We suggest a congruence between the prevalence of MO and MA with the statistical properties of the traveling waves' forms, according to which (i) activation of nociceptive mechanisms relevant for headache is dependent upon a sufficiently large instantaneous affected cortical area anti-correlated to both SD duration and total affected cortical area such that headache would be less severe in MA than in MO (ii) the incidence of MA is reflected in the distance to the saddle-node bifurcation, and (iii) the contested notion of MO attacks with silent aura is resolved. We briefly discuss model-based control and means by which neuromodulation techniques may affect pathways of pain formation.

AUTHOR SUMMARY

The key to the genesis of migraine with aura is a traveling wave phenomenon called cortical spreading depression (SD). Migraine is characterized by recurrent episodes, the aura phase usually lasts only about 30 min. Thus, SD is a transient state. During its course, SD massively perturbs the brain's ion homoeostasis. We resolve the puzzling problem why SD does not engulf all of the densely packed excitable neurons by suggesting a well-established pattern formation mechanism of long-range inhibitory feedback. Furthermore, we use cortical feature maps to create plausible initial conditions as perturbations of the homogeneous state. The statistics of occurrences of the different classes has the potential to reproduce epidemiological statistics of different diagnostic forms of migraine such as migraine with or without aura and provides simple answers to some very controversially discussed current questions in migraine research.

INTRODUCTION

The undoubtedly most fundamental example of transient dynamics is the dynamical phenomenon of excitability, that is, all-or-none behavior. Shortly after transient response properties of excitable membranes were classified into two classes[1], it was also explained in a detailed mathematical model how excitability emerges from electrophysiological properties of such membranes in the ground-breaking work by Hodgkin and Huxley[2]. Two features are central and are by no means exclusive to biological membranes but shared by all excitable elements. Firstly, the inevitable threshold in any all-or-none behavior requires nonlinear dynamics. Secondly, the transient response of the system to a super-threshold stimulation eventually has to lead back to a globally stable steady state after some large phase space excursion. This indicates global dynamics, that is, dynamics involving not only fixed points and their local bifurcations but larger invariant sets, for instance periodic orbits that collide with fixed points. An excitable element is in some sense the washed-up brother of the relaxation oscillator: when the threshold vanishes, a single excitable element usually becomes a simpler behaved—and much longer known—relaxation oscillator[3].

In this study, we propose a model for wave patterns with a characteristic shape, size, and duration. These waves are transient responses to confined, spatially structured perturbations of the homogeneous steady state. The homogeneous steady state is globally stable in our proposed reaction-diffusion model because we also introduce an effective inhibitory mean field feedback control. This leads to a new type of local excitability in a spatially extended medium involving disappearing traveling wave solutions as larger invariant sets. Both, the model and the initial conditions are motivated by the pathophysiology of migraine and clinical observations[4–6] and the results are applied to some currently controversial topics[7–9].

We will briefly introduce concepts of excitable elements and excitable media in two-variable reaction-diffusion systems and also the idea of an additional long-range inhibitory feedback that is studied in various other systems outside the neurosciences and also in neural field models. While we also briefly introduce migraine, the view of mi-

[a)] dahlem@physik.tu-berlin.de; https://sites.google.com/site/markusadahlem/

graine as a dynamical disease is more elaborated in the discussion.

The original conductance-based membrane model from Hodgkin and Huxley, and the more refined versions to date, contain many variables, but fortunately this is not essential for excitable elements. In fact, it turned out that the two classes of excitability are actually amenable to direct analysis in a two-dimensional phase plane by identifying fast and slow processes in the conductance-based model and grouping these into dynamics of just two lump variables[10,11]. Using such a geometrical approach and partly analytical theory, the original empirical classification of excitability was further pursued with bifurcation analysis[12], explaining class I by identifying its threshold as a stable manifold of a saddle point on an invariant cycle and the one of class II as a trajectory from which nearby trajectories diverge sharply (called a canard trajectory). Extensions to these principal mechanisms involve codimension 2 bifurcations and lead also to bursting in three-variable models, which have been investigated in great detail[13]. However, the two-variable models of a fast activator and slow inhibitor and their phase portraits of class I and II became qualitative prototypes for excitable systems in various biological[14], chemical[15] and physical contexts[16].

Distinct from these excitable systems are those that are spatially extended systems, called excitable media. (We use the word "system" as a general term, "medium" only for spatially extended systems, and "element" for point-like systems.) Already the original work by Hodgkin and Huxley[2] described extended tube-like membranes (axons) and introduced the cable equation as a parabolic partial differential equation, which is in the same class as the diffusion equation. Even in reaction-diffusion media with infinite-dimensional phase space, we can again apply geometrical approaches, simply because excitable media are not defined by—in contrast to excitable elements—transient dynamics but traveling wave solutions. The quiescent state is the non-excited homogeneous steady state. And like the quiescent state, excited states of a medium are usually stationary states in some appropriate comoving frame with $\xi = x - ct$. Furthermore, the threshold is related to an unstable stationary state, the critical nucleation solution, usually in another comoving frame including $c = 0$. The existence of the nucleation solution is a simple consequence of multistability, see Fig. 1A, but note that even monostable excitable elements have similar unstable stationary states in class I.

Central to our approach is a distinct subexcitable medium in which localized traveling waves occur only transiently. Reaction-diffusion waves would engulf all of the medium, if formed in a two-variable system with only one activator and one inhibitor with the system's parameters in the appropriate regime. In contrast, localized traveling waves indicate a demand-controlled excitability. Similar ideas to obtain localized traveling, though not transient, waves have been introduced in various contexts, for instance an integral negative feedback or a third, fast diffusing inhibitory component for moving spots in semiconductor materials, gas discharge phenomena, and chemical systems[17–20]. Furthermore, in neural field models[21], localized two-dimensional bumps are studied[22,23] in integrodifferential equations (without diffusion) in the context, for example, of memory

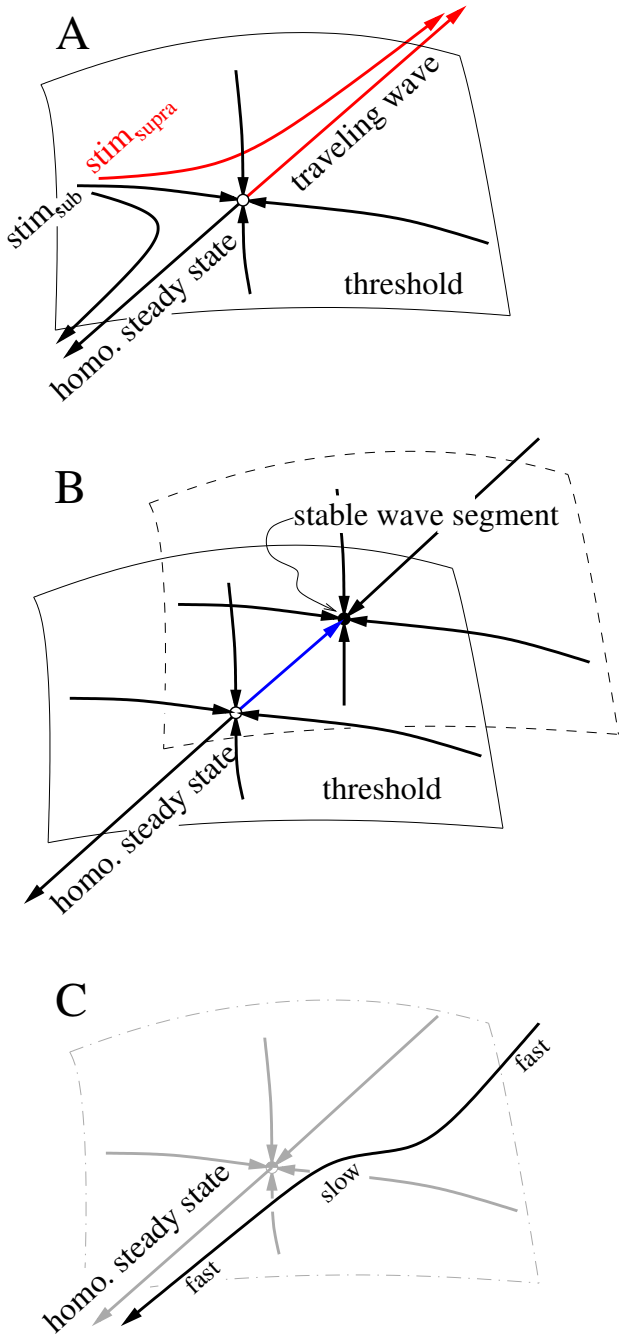

FIG. 1. Schematic sketch of the phase space of (A) the uncontrolled system, (B) the system with mean field control adjusted such that the nucleation solution is stabilized and (C) the system with mean field control and control parameters such that the ghost of the saddle-node bifurcation is still influencing the dynamics.

formation[24]. Localized structures have also been discussed in the context of cortical spreading depression (SD) in migraine before, in particular a model with narrowly tuned parameters that shows transient waves[6,25,26] and a model with mean field feedback control that allows for localized waves[27]. But it is for the first time now that a model is presented in which wave phenomena occur that are both localized and transient, so that a variety of new questions that are controversially discussed in migraine research[7,9,28,29] can be adressed.

Migraine is characterized by recurrent episodes of head pain, often throbbing and unilateral. In migraine without aura (MO), attacks are usually associated with nausea, vomiting, or sensitivity to light, sound, or movement[30]. Migraine with aura (MA) involve, in addition but also rarely exclusively, neurologic symptoms (aura) that are associated with waves of cortical SD[5,31]. SD is a reaction-diffusion process, although, clearly, the originally proposed mechanism of a simple one-variable model for SD front propagation triggered by diffusion of elevated extracellular potassium with bistable kinetics, to date known as Hodgkin-Huxley-Grafstein model[32], does not capture the complex chain of involved reactions[33–35]. However, migraine aura symptoms manifest themselves on a macroscopic scale over several minutes up to one hour and extend over several centimeters when mapped onto the corresponding cortical areas[5,36], see Fig. 2. In this study, we are interested in these clinically relevant properties of migraine with aura. To this end, we exploit the concept of nucleation, growth, and subsequent shrinking of SD in a canonical reaction-diffusion model of activator-inhibitor type with mean field feedback control.

RESULTS

We first present a model constructed by adding a mean field inhibitory feedback to a well known reaction-diffusion system, then we present the statistical properties of the transient behavior this model is exhibiting.

Before infinity and beyond by mean field inhibitory feedback control

The diversity of the behavior of traveling waves in two spatial dimensions was studied in canonical models (see Discussion) depending on the two generic parameters β and ε in Eqs. (1)-(2), which determine the parameter plane of excitability[37]. Eqs. (1)-(2) determine an excitable medium without feedback control. In those media, patterns of discontinuous (open ends) spiral-shaped waves are used to probe excitability and these patterns are closely related to the discontinuous, localized transient waves we propose in our model.

We make use of the fact that at a low critical excitability, called the rotor boundary ∂R_∞, spiral waves do not curl-in anymore but become half plane waves[38,39]. Beyond the rotor boundary lies the subexcitable regime in which discontinuous waves start to retract at their open ends and any discontinuous wave is transient and will eventually disappear. The border ∂R_∞ marks a saddle-node bifurcation at which discontinuous waves collide with their corresponding nucleation solution. This leads to the key idea of our model. A linear mean field feedback control moves this saddle-node bifurcation towards distinct localized wave segments with a characteristic form (shape, size) and behind this bifurcation these waves become transient objects (see Fig. 1).

Before we introduce the effect of mean field feedback control, we have to consider the behavior of continuous waves (closed waves fronts without open ends) when the excitability is decreased. This will be important if we want to understand the fate of any solution, discontinuous or not, under mean field feedback control. Unbroken plane waves propagate persistently even if the parameters are chosen in the subexcitable regime until the propagation boundary ∂P is reached. At this border, the medium's excitability becomes too weak for continuous plane waves to propagate persistently. The border ∂P in parameter space indicates again a saddle-node bifurcation at which a planar traveling wave solution collides with its corresponding nucleation solution. Note, that the planar wave is essentially a pulse solution in 1D and the nucleation solution in 1D is called the slow wave[40].

In Fig. 3A, both the rotor boundary ∂R_∞ and the propagation boundary ∂P are shown in a bifurcation diagram for the excitable medium described by Eqs. (1)-(2). We chose β as the bifurcation parameter and follow (see Methods) the branch of the unstable nucleation solution (NS) whose stable manifold separates the basins of attraction of the homogeneous state and a spiral wave (with two counter-rotating open ends). The unstable manifold of NS consists of the two heteroclinic connections, one to the stable homogeneous state and the other to the traveling wave solution (see Fig. 1). The order parameter on the ordinate in Fig. 3 is the surface area S inside the isoclines at $u = 0$ of the traveling wave solutions, see Eq. (3). We call S the *wave size*.

The mean field control that we introduce by Eqs. (3)-(4) establishes a linear feedback signal of the wave size S to the threshold β. With this linear relation, we introduce two new parameters, the coupling constant K and β_0, the threshold parameter for the medium without an excited state ($S = 0$). Note that the parameter β_0 can be also seen as the sum of two threshold values, the former β in Eq. (2) and an offset coming from the new control scheme. While the introduction of the control introduces two new parameters β_0 and K, at the same time β becomes dependent upon the control, so that we have a total of three parameters. in this study, we kept K fixed at $K = 0.003$ and varied β_0, with a particular focus on the statistics for $\beta_0 \in [1.32,1.33,1.34]$.

We chose β_0 as the new bifurcation parameter in the bifurcation diagram for the full reaction-diffusion model with mean field coupling described by Eqs. (1)-(4), see

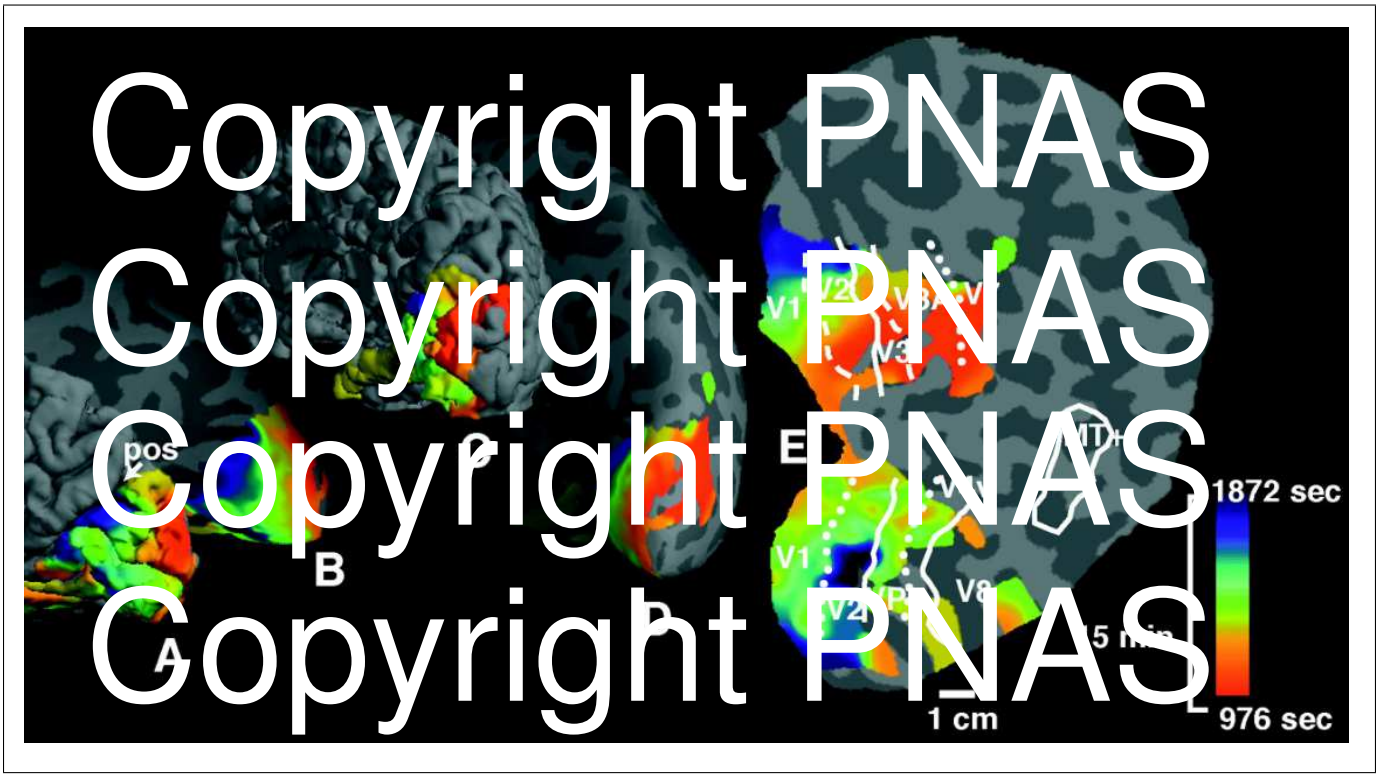

FIG. 2. Source localization of the magnetic resonance (MR) data signal of SD (from[5]). Color code: time from onset, locations showing the first MR signals of SD are coded in red, later times are coded by green and blue (see color scale to the right). Signals from the first 975 seconds were not recorded because the migraine attack was triggered outside the MR imaging facility. (A) The data on folded right posterior pole hemispheric cortex; (B) the same data on inflated cortical surface; (C and D) the same data shown on the entire hemisphere from posterior-medial view (oblique forward facing), folded and inflated, respectively. As described in the original study[5], MR data were not acquired from the extreme posterior tip of the occipital pole (rearmost portion). (E) A fully flattened view of the cortical surface. The aura-related changes are localized wave segments. Note that in the flattened cortex was cut along the steep sulcus calcarine to avoid large area distortions induced by the flattening process. The colored border to the left is the cut edge that should be considered being connected such that the color match up as seen in (B and D). (Copyright permission from authors granted, from PNAS is requested.)

Fig. 3B. This diagram is a sheared version of the one without mean field coupling in Fig. 3A. While it is a trivial fact, that the linear relation in Eq. (4) describes an affine shear of the axises (β, S) of bifurcation diagram in A to the axises (β_0, S) in B, the fact that the branch of the NS solution can be mapped this way is not. Firstly, this relies on the way we introduce the feedback term. It just adds a constant value to the old bifurcation parameter β, if the solution under consideration is stationary. Therefore, any stationary solution must exist in both diagrams being just sheared branches. The same holds true for traveling wave solutions that are stationary in some appropriate comoving frame $\xi = x - ct$ with speed c. However, not much can be said about the stability of such solutions, when we introduce the mean field feedback term.

The branch of the formerly unstable nucleation solution NS (Fig. 3A) folds in Fig. 3B such that two solutions coincide for a given value of β_0 until they collide and annihilate each other at a finite value of $S \approx 5.5$ for $K = 0.003$. For the fixed value of $K = 0.003$, the upper branch is a stable traveling wave solution in the shape of a wave segment, while the lower branch is the corresponding nucleation solution of this wave segments, as schematically shown in Fig. 1B. The fact that the upper branch is stable was confirmed by numerical simulations. Larger K, that is, a less steep control line in Fig. 3A can be seen as a "harder" control, because a small given change in S leads to larger variations in the effective parameter β. As a consequence, it is difficult to continue by means of this control the lower part of the branch corresponding to small traveling wave segments in numerical simulations.

The choice of a parameter regime for this model that shows transient localized waves and is globally stable with the homogeneous state as the only attractor is now straightforward. Transient localized waves occur due to a bottleneck—or ghost behavior—after the saddle-node bifurcation.

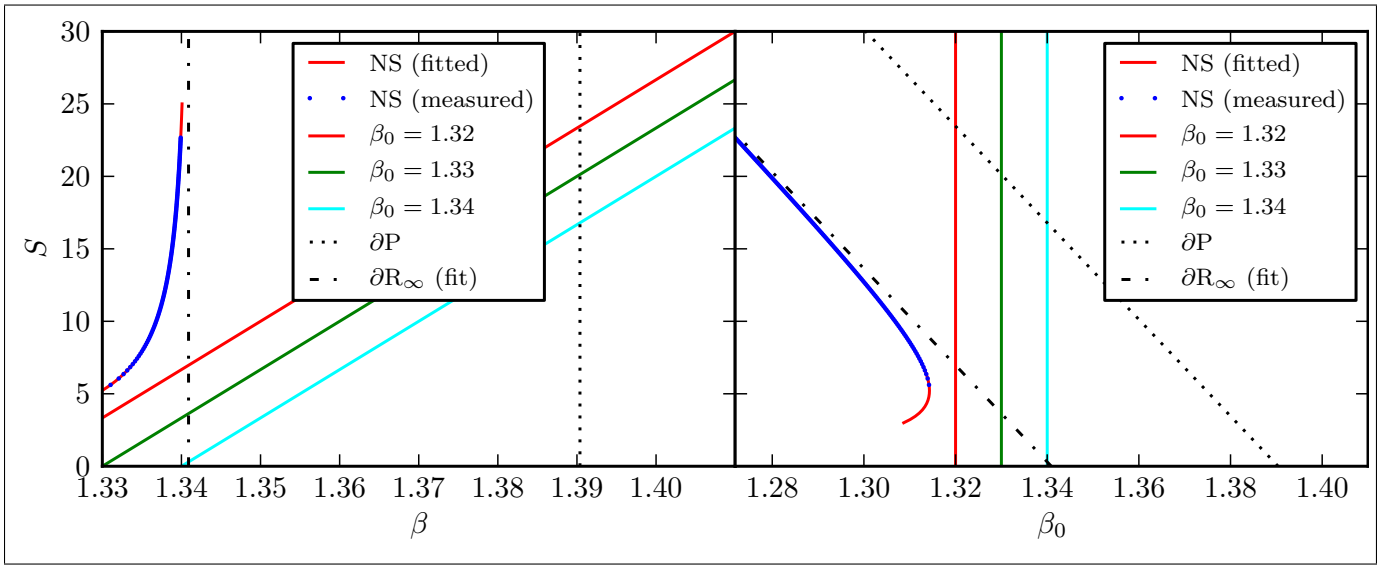

FIG. 3. **(left) The S - β plane** with nucleation solution NS , propagation boundary ∂P, rotor boundary ∂_{R_∞} and control lines for the used values of β_0. **(right) The S - β_0 plane** with the same quantities.

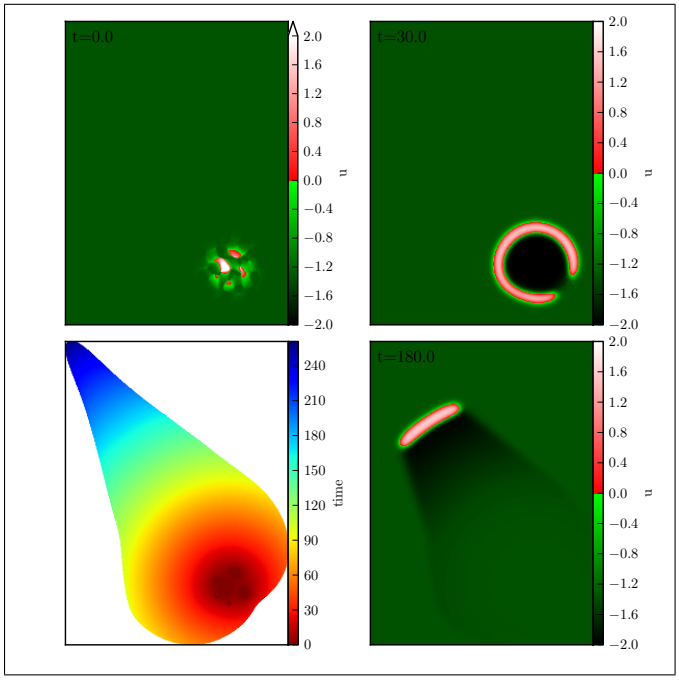

FIG. 4. An example of a transient solution. Initial conditions, i.e. activator concentration u at $0s$ (upper left), snapshot of activator-concentration u after $30\,s$ (upper right), after $180\,s$ (lower right). Time of passing through threshold value $u_0 = 0$ from below the first time, i.e. passing of the wave front (lower left).

Statistical properties

To examine the typical transient patterns that the system generates, we want to know how the system responds to arbitrary initial conditions with the noticeable constraint that the system should initially be in the homogeneous steady state almost everywhere and the arbitrary perturbations from it are localized. As it is not possible to formulate an analytical solution to the equations for arbitrary initial conditions, the idea is to simulate the dynamics for (many) different initial conditions. Ideally, these initial conditions should be "equally spaced" in phase space, in order to obtain relevant statistics about the different evolution possibilities. The problem that arises at this point is that an initial condition of this system is not only living in an infinite dimensional space (an initial condition would be given by two C^2-functions $\mathbb{R}^2 \to \mathbb{R}$) but because of the nonlinearity of the equations, the set of all solutions is not even a vector space. To our knowledge, there is no helpful mathematical structure that could guide us in choosing our initial conditions. To attack this problem, we take a set of patterns, which are parameterized by a finite number of parameters and scan through these parameter. For details on the patterns see Methods.

Of course, in characterizing the solutions, the same problem arises and appropriate characteristic parameters for the solutions have to be defined.

To explain the three parameters we have chosen for the solutions and why they suit this problem, it is helpful to have a look at the lower left part of Fig. 4, in which an example solution is displayed. The first parameter we choose is the maximal area in which such a solution has activator concentration over a certain threshold level at

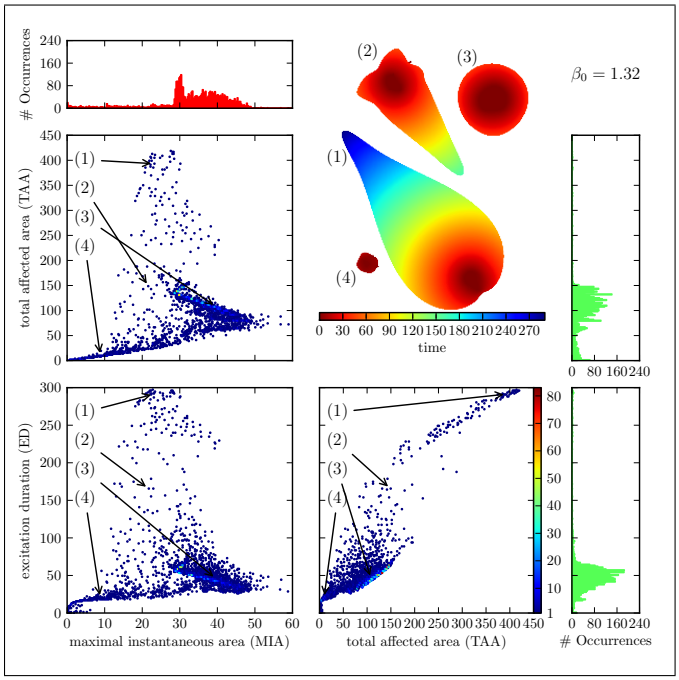

FIG. 5. **Distribution of solutions** for the control close to ∂_{R}.

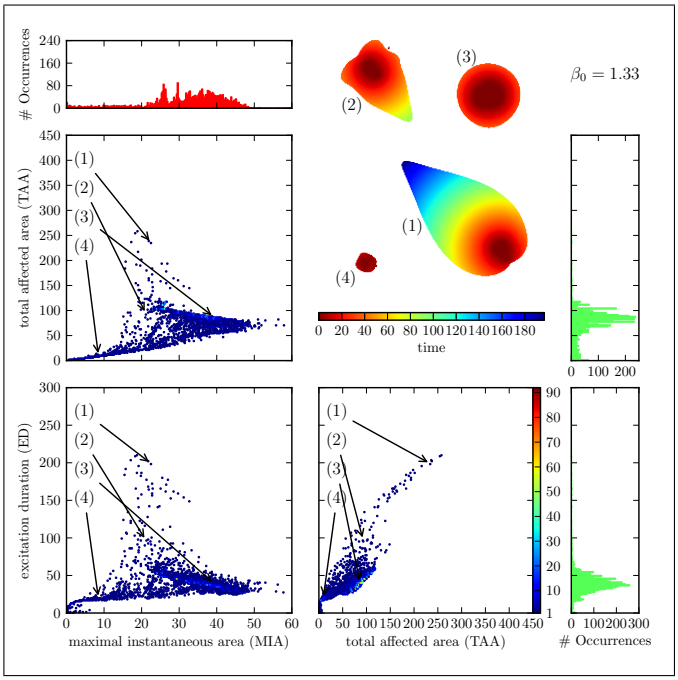

FIG. 6. **Distribution of solutions** for the control line at an intermediate distance to ∂_{R}.

one instant of time, termed maximal instantaneous area (MIA). The threshold level is taken to be $u = 0$, although this is the same threshold as used to define S, this is rather convenience than necessity. The second parameter is the total area that has experienced an activator concentration above this level at some time during the course of the solution, termed total affected area (TAA). The third parameter is the time, during which the area of activator concentration above threshold is non-zero, termed the excitation duration (ED). Of course, the exact value of all these parameters for one single solution depends on the choice of threshold. For once, the threshold value has to be chosen such that after the activator concentration has fallen below it, no secondary excitation will be generated.

The example solution depicted in Fig. 4 is a comparatively long lived solution. It starts out very symmetrically (circularly) shaped, at one instant of time it breaks open into a discontinuous wave and a shape of the front develops, which is similar to that of a particle-like wave but because of the chosen control parameters, it shrinks in time and vanishes in the end. Because at the point when the circle breaks open, a comparatively large area is affected, it takes some time until it vanishes and the resulting TAA is relatively large. So this example solution has large ED, large MIA and large TAA. If the circle had not broken open at all, the control would have made the threshold value very large and the solution would have collapsed very quickly because of the propagation boundary ∂P, such that the ED and the TAA would have been short, whereas the MIA would have been large. Other prototypical courses of solutions take place for instant, when the initial conditions affect the activator over a larger area but only in the middle of the area, the value is high enough to start a solution. In the surrounding area, the activator level is not high enough for that but the increased activator concentration leads to a rise in inhibitor concentration until the time the front reaches those parts and as a consequence, the solution vanishes early, having small ED, small TAA and small MIA as a consequence.

We did the simulation for three different adjustments of the control force, successively going farther and farther away from the bifurcation point. Each of these simulations were started using 8000 initial conditions generated in a manner that is described in Methods. Each of these initial conditions resulted in a solution that was classified according to the three parameters mentioned above. The solutions that did not result in any excitation at all (ED=MIA=TAA=0) were discarded. The density plots according to the classification parameters are shown in Figs. 5, 6, 7. First of all, though the distribution of the solutions varies significantly, the number of solutions that represent an excitation hardly varies at all (4171 for small, 4183 for intermediate, 4182 for large distance from the bifurcation point), the symmetric difference between the sets of initial conditions that lead to an excitation contains between 5 and 19 solutions. From this we can also deduce that the set of initial conditions that lead to an excitation does not significantly depend on the choice of control parameters.

When looking at Fig. 5 one notices a clustering of

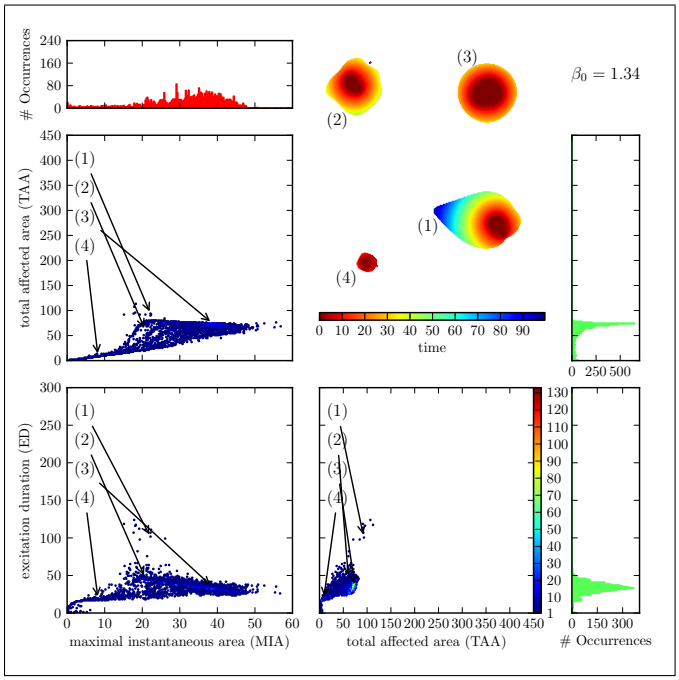

FIG. 7. **Distribution of solutions** for the control far away from ∂_{R}.

the solutions in certain regions of the classification parameters. In the section that depicts the TAA against the MIA, we notice three coarse clusters. Cluster I, the largest with high MIA and comparatively low TAA; cluster II, one that is less populated with low MIA and low TAA; and cluster III, one that is very sparsely populated with intermediate MIA and high TAA. The boundaries between these clusters are not very sharp. One could think that a solution that affects an overall large area (high TAA) will also affect a large area at one instant of time (high MIA). From looking at the mentioned clusters, one sees that this is not the case, the solutions with the highest MIA have all comparatively low TAA (clusters I and II) and the ones that have a high TAA only achieve an intermediate MIA (culster III).

A partial explanation for this can be read off from the depiction of TAA against ED. All solutions that have a large TAA are also solutions that have a large ED, i.e., cluster III is distinct also in this plane. More than that, the dependence seems to be almost linearly. This is reminiscent of the localized particle-like wave solutions. For these, the area that is affected grows linearly in time because the area that these solutions occupy at one instant of time is constant.

The two clusters I and II that we observed merge to one in this plane of projection because they differ only very little in ED. This can also be noted, when comparing the planes MIA vs. TAA and MIA vs. ED, also here the cluster III with high TAA translates to a cluster with high ED and the cluster I with high MIA and comparatively low TAA moves closer to cluster II with both low ED and MIA.

When varying the β_0 parameter of the control force, the distribution of solutions in MIA-TAA-ED-space changes drastically. Upon raising the β_0 parameter from $\beta_0 = 1.32$ over $\beta_0 = 1.33$ to $\beta_0 = 1.34$, the system is put more and more into the subexcitable regime and the solutions are less and less affected by the ghost behavior (saddle-node bifurcation), see Fig. 3. This is noticeable by observing that the cluster with high TAA / high ED becomes less pronounced and vanishes almost completely for $\beta_0 = 1.34$. This can be understood as an interplay between the mean value of MIA in cluster III at about 25 and S at the propagation boundary (at ∂P, $S \approx 24$, $S \approx 20.75$, and $S \approx 17.5$ for $\beta_0 = 1.32$, $\beta_0 = 1.33$, and $\beta_0 = 1.34$, respectively). For the control line farthest away from the saddle-node bifurcation ($\beta_0 = 1.34$), ∂P is below even the smallest values of MIA in cluster III. Note that the value of S at the ghost is about 6, well below the propagation boundary. Also the other two clusters merge though there still exist solutions with high and with low MIA, but the transition is much more fuzzy than it was before.

In Figs. 5, 6 and 7, we have included a little 'bestiary' to illustrate the typical courses of solutions in the respective clusters and their change upon varying the parameter β_0, the initial conditions for solutions 1-4 in these figures are always the same. From this arbitrarily chosen selection, we see that the MIA of each solution hardly changes between the β_0 values. Whereas the change of TAA and ED always go hand in hand and—depending on the cluster—can be up to fourfold for the chosen range of β_0.

One could argue that the formation of clusters is an artefact of the choice of initial conditions. There is no simple answer to this. As mentioned, it is not possible to examine the complete set of initial conditions. Neither does this set carry a helpful structure which would allow a sensible 'equidistant' sampling. This is the reason why we made the mentioned choice of initial conditions. For testing purposes, we also tried different schemes for the generation of initial conditions and found the same distribution of clusters qualitatively.

In Fig. 8, we have plotted the cumulative distribution functions for the three classification parameters and the three choices of mean field control. From this picture we see, that the distribution of the MIA is only hardly influenced by the choice of control. This is very different for TAA and ED. For the TAA for example there are values (around 75), where for one choice of control the majority of solutions is below and for another choice the majority is above. For example, the fraction of values below TAA=80 is 0.995 for $\beta_0 = 1.34$ and 0.216 for $\beta_0 = 1.32$. Also, we see that the cumulative distribution function for the TAA converges to 1 much slower, the closer the control is to the saddle-node bifurcation. This means, that more solutions with high TAA exist for these choices of control.

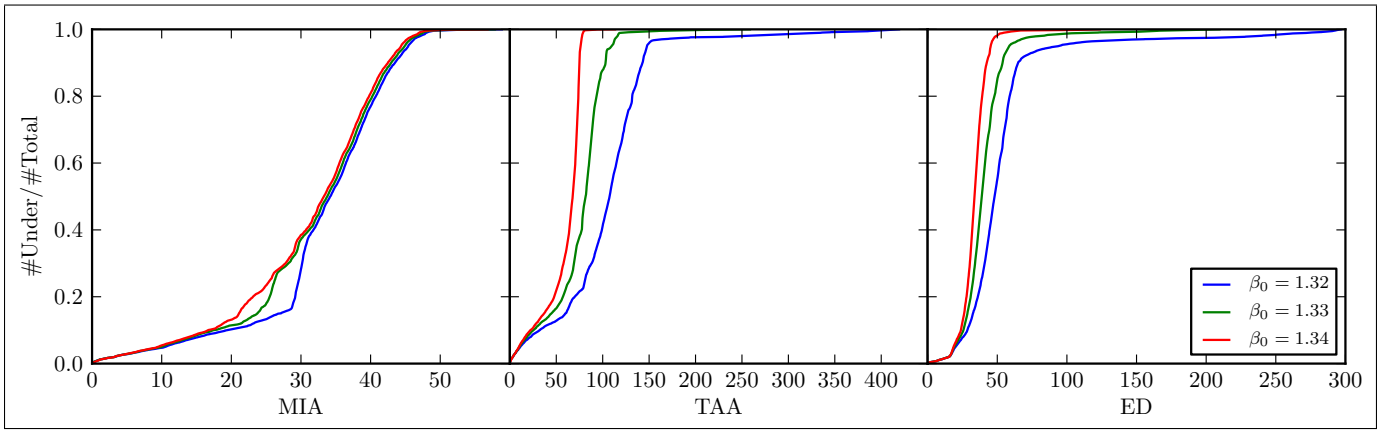

FIG. 8. **Cumulative distribution functions** for the different classification parameters.

DISCUSSION

In this section we discuss three subjects related to the intended application to migraine pathophysiology. Firstly, the possible congruence between the prevalence of migraine subforms with the statistical properties of the wave patterns we observed; secondly, the possible physiological origin of the inhibitory feedback control; and thirdly, novel therapeutic approaches. We start with a discussion of the approach of using a canonical model.

Canonical model and generic parameters for weakly excitable media

More realistic models of SD are given by a conductance-ion-based models of SD[41–43] with up to 29 dynamics variables. The fast inhibitory feedback that we suggest can be modeled in addition by neural field models[21]. Such large-scale models of brain structure, including lateral connectivity, are available but still require enormous computer capabilities. We will argue here, in which sense our model is canonical for the problem we attack.

Generally speaking, an excitable medium is a spatially extended system with a stable homogeneous steady state being the quiescent state and one or many excited states that develop after a sufficient perturbation from the quiescent state (Fig. 1A). The excited states are traveling wave solutions that propagate with a stable profile of permanent shape (possibly with some temporal modulation, such as breathing or meandering). To study generic features of an excitable medium, the simulations are often carried out in the reaction-diffusion system given by Eqs. (1)-(2), the popular FitzHugh-Nagumo kinetics. Originally, the FitzHugh-Nagumo kinetics were a caricature of the electrophysiological properties of excitable membranes[44,45], but these equations with $D = 0$ became a canonical model of *local* excitability of type II (based on Hopf bifurcation, either supercritical with subsequent extremely fast transition to a large amplitude limit cycle, named canard explosion[46], or subcritical[47]), and also, for $D \neq 0$, of *spatial* excitability[37], sometimes including diffusion in the second inhibitory species, which we do not consider here. Because we are considering transient behavior originating from a high threshold regime (towards weak excitability), the classification of local excitability in type I and II (based on the transition at vanishing threshold, i.e., into the oscillatory regime) is not relevant. Furthermore, it is not clear whether this classification carries over in a meaningful way to the dynamics of spatially extended systems.

We consider the set of Eqs. (1)-(2) as canonical for two reasons. First, because the activator Eq. (1) has the simplest polynomial form of bistability. Note that Eq. (1) was for this reason originally suggested by Hodgkin and Huxley as the first mathematical model of the potassium dynamics in SD. It was published by Grafstein, who also provided experimental data supporting such a simple reaction-diffusion scheme for the front dynamics[32]. Second, the inhibitor Eq. (2) has a linear rate function, in fact, the rate function is only of a function of the activator u. This is the simplest inhibitor dynamics needed for pulse propagation. By neglecting an additional linear term $-\gamma v$ in the inhibitor rate function, we limit the origin of excitability to the case of a supercritical Hopf bifurcation with subsequent canard explosion and avoid the bistable regime that exits in the subcritical case. The subcritical Hopf bifurcation occurs only in a narrow regime when γ is close to 1 and β close to 0. We have tested some simulations with $\gamma = 0.5$ with similar results.

As a consequence of our assumptions about the model being in this canonical form, only two parameters exits, β which is associated with the threshold and the ε, the time scale separation of activator and inhibitor dynamics. Of course, the choice of parameters can be quite different, a common choice is α in the cubic rate function $f(u) = u(u-\alpha)(u-\alpha)$ but there are only two free

parameters or two equivalent groups of parameters. So there are the same bifurcations in the parameter planes (ε, β) or (ε, α), but to map the dynamics between equivalent groups of parameters might involve changes in time, space and concentrations scales.

In particular the question of how the incidence of MA is reflected in the distance to the saddle-node bifurcation, involves a measure on the parameter space, which we have suggested to get from pharmacokinetic-pharmacodynamic models[26].

Application to migraine pathophysiology

The cause of the neurological symptoms in migraine with aura (MA) is the phenomenon of cortical spreading depression (SD)[5,31,48,49]. Whether SD is also a key to the subsequent headache phase is an open question, in particular, in cases of migraine without aura (MO). If SD occurs in MO, it must remain clinically silent[7,8] or—by definition of diagnostic criteria—neurological symptoms must last less than 5min. Of course, the transient nature of SD poses challenging problems in clinical observability, in particular for objective measures by means of non-invasive imaging when clinical symptoms do not even indicate the aura phase with SD. The aura is usually, though not always, before the headache phase. Attacks observed with non-invasive imaging are usually triggered, which also could cause a trigger-specific bias. One well-documented case of a spontaneous migraine headache supports the contested notion of 'silent aura', because blood-flow changes where observed that were most likely the result of SD[50].

We suggest a qualitative congruence between the prevalence of MO and MA with the statistical properties we found in the transient response properties. We do not suggest that all MO attacks are related to SD nor that pain formation in MA is exclusively caused by SD. Rather that SD is one pathway of pain formation in MO and MA. We refer to this pathway as the "spreading depression"-theory of migraine[49]. The "migraine generator"-theory (MG), a dysfunction in a central pattern generator in the brainstem that modulates the perception of pain, is for various reasons not less plausible[9]. Some of the seemingly conflicting and controversially discussed evidence is probably resolved when one considered the basis of the classification of migraine. We currently have a symptom-based classification for migraine with possibly overlapping etiologies for individual subforms. In the light of an etiology-based classification with possibly overlapping symptoms the conflicts seem less puzzling to us. We also need to investigate an interplay of SD and MG, namely to which degree MG modulates pain traffic from SD generated in the intracranial tissues.

The cortex is not pain sensitive. There are detailed investigations how SD in the cortex can cause pain via pain sensitive intracranial tissues and subsequent activation in the trigeminal nucleus caudalis in the brainstem[51,52], but cf.[53,54]. The qualitative congruence between the prevalence of MO and MA with the statistical properties we found in the transient response properties is based on the following assumption on the geometrical layout: In the initial phase of cortical SD, with increased blood flow (hyperemic phase), a local release of noxious substances (ATP, glutamate, K^+, H^+) are thought to diffuse outward in the direction perpendicular to the cortex into "the leptomeninges resulting in activation of pial nociceptors, local neurogenic inflammation and the persistent activation of dural nociceptors which triggers the migraine headache"[55], but for issues concerning the blood brain barrier system cf.[56]. If diffusion vertical to the affected area is critical, size and shape of this area should play a critical role, see Fig. 9. This suggests that SD waves activate nociceptive mechanisms dependent upon a sufficiently large instantaneously affected cortical area, i.e., large MIA.

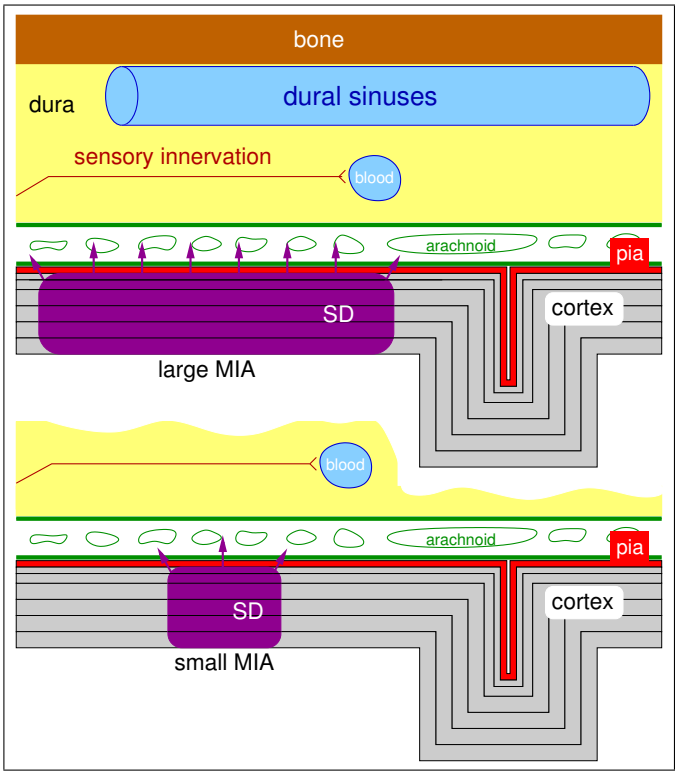

FIG. 9. **Schematic representation of cross section of cortex, meninges and skull.** The leptomeninges refer to the pia mater and arachnoid membrane. SD releases noxious substances with increased blood flow thought to diffuse outward. Activation of pain pathways can depend on MIA.

The aura phase on the other hand must clearly correlate with long and large enough cortical tissue being affected to notice the neurological deficits. In particular, because the very noticeable visual symptoms often start where the cortical magnification factor is large, so that only if they move into regions of lower magnification they get magnified by the reversed topographic mapping[25].

The seemingly contested notion of MO (migraine without aura) with silent aura is also resolved.

A view at the connection between MIA and TAA as well as MIA and ED in our model is shown in Fig. 10. It shows that in the range of high MIA the average values for TAA and ED are becoming smaller. From Fig. 10 we can also read off that the range with the most events is in the regime of relatively high MIA (around 30) and significantly after the peak of ED resp. TAA. Moreover in the range with most events, the correlation coefficient r(MIA, ED) is always negative and the correlation coefficient r(MIA,TAA) is mostly negative. All these effects are stronger, the closer the control line is located to the saddle-node bifurcation.

From these statistical correlations between MIA and TAA resp. ED and the distribution of the number of events, one could speculate that cases of MA are more rare and the quality of the headache in these cases might be less severe. This is exactly what has been reported in the medical literature[57].

While the number of events with high ED and high TAA is influenced by the distance of the control line to the saddle node bifurcation, the number of events with high MIA is much lesser affected. So in a way, the distance to the saddle node bifurcation controls the prevalence of MA in our model, while the prevalence of MO is not much affected.

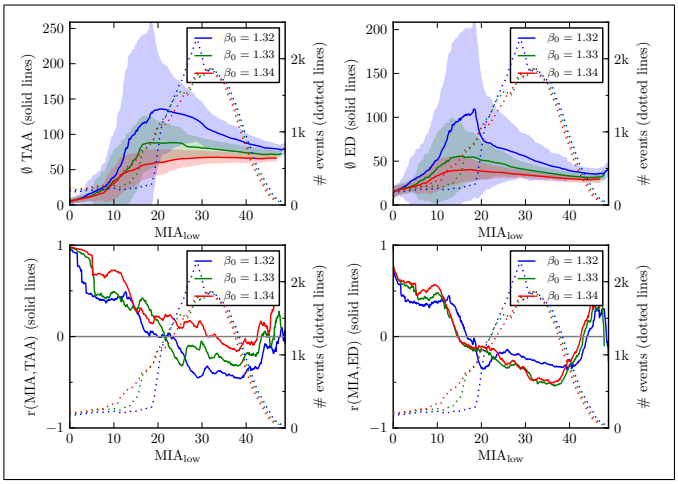

FIG. 10. **Statistical analysis of output data.** For all four pictures we took all data points with MIA in the interval [$\mathrm{MIA_{low}}$, $\mathrm{MIA_{low}}$+10] ("sliding window") and analyzed the connection with TAA **(left column)** and ED **(right column)**. In the **(upper row)**, the average value is plotted with *solid lines*, the area of one standard deviation around this value is shaded. In the **(lower row)**, the correlation coefficient between MIA and the respective quantity is plotted. In all plots, the *dotted lines* indicates the number of events for the respective interval with $\mathrm{MIA_{low}}$.

Inhibitory feedback and neurovascular coupling

This naturally rises the question of the physiological origin of the inhibitory feedback control. The hyperemic phase engulfs large regions of the human cortex[31], while we suggest in this study the homeostatic breakdown directly due to SD is much more limited in extent. A fast spreading increased neural activation in adjacent cortical areas could represent synaptic activation through feedforward and feedback circuitry. This was suggested by Wilkinson[58]. This would in turn extend the area of the hyperemic phase towards tissue that is not yet recruited into the SD state and this mechanism has therefore a neuroprotective effect by an increased blood flow which we mimic by the inhibitory mean field feedback.

The coupling between neural activity and subsequent changes in cerebral blood flow, called neurovascular coupling, has a significant time delay in the order of seconds, which we ignore for the sake of simplicity in our model.

Model-based control by neuromodulation

We briefly discuss model-based control and means by which neuromodulation techniques may affect pathways of pain formation and the aura phase.

The emerging transient patterns and their classification according to size and duration offer a model-based analysis of phase-dependent stimulation protocols for non-invasive neuromodulation devices, e.g. utilizing transcranial magnetic stimulation (TMS)[59], to intelligently target migraine. For instance, noise is a very effective method to drive the system back into the homogeneous steady state more quickly. In general, responses of nonlinear systems to noise applied when the system is just before or past a saddle-node bifuraction are well studied. Before the saddle-node on limit cycle bifuraction, the phenomenon of coherence resonance (CR) describes that a certain amount of noise makes responses most coherent[60]. Behind the saddle-node bifurcation on a limit cycle the time the flows spend in the bottleneck region of the ghost is shortened[61]. However, noise would, according to our model, mainly positively affect ED and TAA, that is, the aura, while it could even worsen the headache, if applied early during the nucleation and growth process. Therefore, TMS using noise stimulation protocols, which is currently considered, should be applied only some time after first noticing aura symptoms.

Headaches are not generally considered appropriate for invasive neurosurgical therapy, but when all else fails—preventives, abortives, and pain management—invasive brain stimulation techniques are also considered, e.g. occipital nerve stimulation (ONS)[62,63]. So model-based control will become increasingly important. Also the importance of modeling related epileptic seizure dynamics as spatio-temporal transient patterns, has been suggested in a recent paper[64]. Model-based control of Parkinson's disease, is already considered, yet Schiff remarks quite correctly[65]: "It seems incredible that the tremendous

body of skill and knowledge of model-based control engineering has had so little impact on modern medicine. The timing is now propitious to propose fusing control theory with neural stimulation for the treatment of dynamical brain disease."

We suggest to consider migraine as a dynamical disease that could benefit from model-based control therapies.

METHODS

As a generic model for our excitable medium we use the well known FitzHugh-Nagumo equations[66], augmented by a diffusion term for the activator variable:

$$\varepsilon \frac{\partial u}{\partial t} = u - \frac{1}{3}u^3 - v + \nabla^2 u \tag{1}$$

$$\frac{\partial v}{\partial t} = u + \beta. \tag{2}$$

The parameter ε separates the timescales of the dynamics of the activator u and the inhibitor v. ε is taken to be small. In the present work, we use a value of $\varepsilon = 0.04$. The parameter β is a threshold value which determines from which activator level on the inhibitor concentration is rising. The local dynamics of (2) (i.e. without the diffusion term) is oscillatory for $|\beta| < 1$ and excitable for $|\beta| > 1$. At $|\beta| = 1$ the local dynamics undergo a supercritical Hopf-bifurcation. We choose a value of $\beta = 1.1$ throughout this work. To integrate (2), we used a simulation based on spectral methods[67] and adaptive timestepping.

We define the (instantaneous) wave size as the area with activator level u over a certain threshold u_0:

$$S(t) := \iint \Theta\left(u(x, y, t) - u_{\text{threshold}}\right) \mathrm{d}x\mathrm{d}y, \tag{3}$$

where Θ is the Heaviside function and $u_{\text{threshold}} = 0$.

Equations (2) are a paradigmatic model of an excitable medium[68]. It possesses a stable homogeneous solution as well as stable excited states (pulses, spirals or double spirals) cf.[27,69] The boundary separating the basins of attraction of these types of solution consists of unstable so-called 'nucleation-solutions', which are areas of excitation which are traveling at uniform speed. The size in the sense of (3) of these solutions is plotted against the parameter β in Fig. 3. To measure this line ∂_{R}, called the 'rotor boundary', we used a pseudo-continuation procedure. Which is described below.

Making the parameter β dependent on the wave size S adds a mean field control to the system.

$$\beta = \beta(t) = \beta_0 + K \cdot S(t), \tag{4}$$

where K, S_0 and β_0 are control parameters.

If the control line defined by (4) intersects ∂_{R}, the point of intersection with higher S is stabilized, cf.[18].

The aim of the present work is to shed light on the transient behavior, occurring when the control line (4) is close to ∂_{R} but does not intersect it.

To account for the imprecision in the rotor boundary of the simulation and the exact rotor boundary ∂_{R}, we measured the rotor boundary in our simulation using a pseudo-continuation procedure. For this, we set the control such that it intersects ∂_{R} and thus stabilize an otherwise unstable solution on it. Letting the simulation run until the system has stopped fluctuating, saving the (β,S)-pair, changing the control slightly and doing things over yields points of ∂_{R} in our system. From this measured ∂_{R} and the propagation boundary, inferred from continuation in 1D, we chose 3 suitable control lines which were used for simulations in this work:

$$\begin{aligned} K &= 0.003 \\ \beta_0 &\in [1.32, 1.33, 1.34] \end{aligned} \tag{5}$$

For the purpose of visualization of the saddle-node bifurcation occurring in the bifurcation diagram of the system with mean field control (right of Fig. 3, we fitted the measured branch of nucleation solutions to a function of the form $\beta = a + \frac{b}{cS+S^2}$ which also allows us to obtain an approximation for the β value of the rotor boundary $\partial \mathrm{R}_\infty$.

As mentioned in section , we need an appropriate sampling of initial conditions for (2), ideally being equidistantly sampled in some distribution. As was also mentioned, the set of all initial conditions for this system does not—to our knowledge—carry a helpful mathematical structure which allows us to achieve this aim easily. In order to attack this problem, we turned to the physiological origin for that we chose this model.

A set of initial conditions should naturally reflect plausible spatial perturbations of the homogeneous steady state of the cortex. This can be achieved by defining localized but spatially structured activity states on large-scales, i.e., on the order of millimeters. Such pattern are obtained from cortical features maps (see Fig. 11) by sampling three parameters (*scaling*, *depth*, and *size*) that define patches of lateral coupling in theses maps. A fourth parameter (*excess*) determines the amplitude of the perturbation. In the following, we first describe the rational behind using a cortical feature map and then the sampling.

We focus on a cortical feature map in the primary visual cortex (V1) called pinwheel map. V1 is located at the occipital pole of the cerebral cortex and is the first region to process visual information from the eyes. Migraine aura symptoms often start there or nearby where similar feature maps exist.

In V1, neurons within vertical columns (through the cortical layers) represent by their activity pattern edges, enlongated contours, and whole textures "seen" in the visual field. This representation has a distinct periodically microstructured pattern: the pinwheel map. Neurons preferentially fire for edges with a given orientation and the preference changes continuously as a function of cortical location, except at singularities, the pinwheel centers, where the all the different orientations meet[70,71].

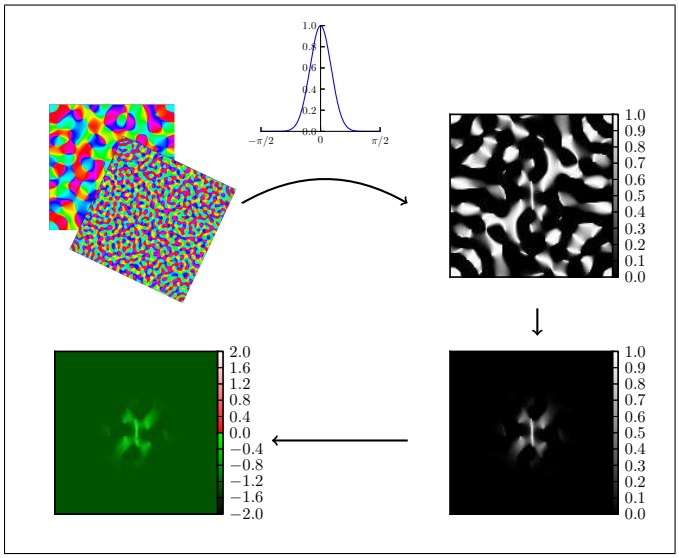

FIG. 11. To construct initial conditions from artificially generated pinwheel maps, we first took such a pinwheel map with a certain *scaling* (upper left), then we chose a selection of excited orientations by means of a gaussian. The width of the gaussian gives the selection *depth* (upper right). After that, we masked the result spatially with another gaussian distribution that is radially symmetric (lower right). The width of this gaussian gives the third parameter, the *size* of the pattern. Finally the result is scaled, giving rise to the fourth parameter, we called the *excess* and added to the activator variable in the homogeneous state (lower left). The inhibitor variable is put into the homogeneous state.

Iso-orientation domains form continuous bands or patches around pinwheels and, on average, a region of about $1\,\mathrm{mm}^2$ (hypercolumn) will contain all possible orientation preferences. This topographical arrangement allows one hypercolumn to analyze all orientations coming from a small area in the visual field, but, as a consequence, the cortical representation of continuous contours in the visual field would be depicted in a patchy, discontinuous fashion[72]. In general, spatially separated elements are bound together by short- and long-range lateral connections. While the strength of the local short-range connection within one hypercolum is a graded function of cortical distance, mostly independent of relative orientation[73], long-range connections over several hypercolums connect only iso-orientation domains of similar orientation preference[74,75]. Even nearby regions, which are directly excitatory connected, have an inhibitory component through local inhibitory interneurons and this is likely be used to analyze angular visual features such as corners or T junctions[73].

Given the arguments above, we can now obtain localized yet spatially structured activity states on the scale we aim for as initial conditions by using iso-orientation domains that form continuous patches around pinwheels and extend in a discontinuous fashion over larger areas.

In[76] the authors analyzed the design principles that lie behind the columnar organization of the visual cortex. The precise design principles of this cortical organization is governed by an annulus-like spectral structure in Fourier domain[70,76], which is determined by mainly one parameter (*scaling*), that is, the annulus width. The parameter *depth* reflects the tuning properties of orientation preference or we can also interpret this as the range of orientation angles that we consider within the iso-orientation domain. The third parameter reflects the distance long-range coupling ranges before it significantly attenuates.

These design principles can be exploited and a procedure can be designed to construct maps with the same properties. The constructed maps come very close to the maps found in brains of macaque monkeys (see[76] and references therein).

To construct initial conditions from these maps we used a procedure that uses four control parameters and is visualized in Fig. 11. The details are as follows: A pinwheel map is a function that maps our twodimensional plane to the interval $(-\pi/2, \pi/2]$. We construct such a map using the procedure in[76]. During construction, we can choose the *scaling* of the map. This is our first parameter. After constructing this map, by means of a gaussian, we choose a range of orientations that is excited. Mathematically speaking this is the concatenation of the gaussian distribution with the pinwheel map. This gives the next parameter, namely the width of the gaussian that selects the angles, we call that parameter the *depth*. The next step is to constrain the generated pattern spatially by multiplication with another gaussian which is defined on the plane P and chosen to be rotationally symmetric. The width of this gaussian gives rise to the third parameter, the *size* of the pattern. Finally we multiply the pattern by a certain amplitude, which is chosen such that the integral of the pattern over the plane gives a chosen number, which constitutes the fourth parameter, we called the *excess*.

Finally, initial conditions are generated by setting the plane to the (stable) homogeneous state and then adding the generated pattern to the activator variable u.

In a first run, we scanned the space spanned by the four parameters coarsely. We used the marginal distributions of the number of solutions with ED> 0 with respect to the parameters to decide how densely to sample the parameter space in the final run.

ACKNOWLEDGMENTS

The authors kindly acknowledge the support from the Deutsche Forschungsgemeinschaft (DFG) in the frameworks of SFB910 and GRK1558, and from the Bundesministerium für Bildung und Forschung under grant BMBF 01GQ1109. MD has been supported in part also by the Mathematical Biosciences Institute at the Ohio State University and the National Science Foundation under Grant No. DMS 0931642. The authors would also

like to thank Gerold Baier, Michael Guevara, Zachary Kilpatrick, and Eckehard Schöll for helpful discussions and advice.

REFERENCES

[1] A. L. Hodgkin, "The local electric changes associated with repetitive action in a medullated axon," J. Physiol. **107**, 165 (1948).

[2] A. L. Hodgkin and A. F. Huxley, "A quantitative description of membrane current and its application to conduction and excitation in nerve," J. Physiol. **117**, 500 (1952).

[3] B. van der Pol, "On relaxation oscillations," Phil. Mag. **2**, 978–992 (1926).

[4] M. A. Dahlem, R. Engelmann, S. Löwel, and S. C. Müller, "Does the migraine aura reflect cortical organization," Eur. J. Neurosci. **12**, 767–770 (2000).

[5] N. Hadjikhani, M. Sanchez Del. Rio., O. Wu, D. Schwartz, D. Bakker, B. Fischl, K. K. Kwong, F. M. Cutrer, B. R. Rosen, R. B. Tootell, A. G. Sorensen, and M. A. Moskowitz, "Mechanisms of migraine aura revealed by functional MRI in human visual cortex," Proc. Natl. Acad. Sci. U.S.A. **98**, 4687–4692 (2001).

[6] M. A. Dahlem and N. Hadjikhani, "Migraine aura: retracting particle-like waves in weakly susceptible cortex," PLoS ONE **4**, e5007 (2009).

[7] Cenk Ayata, "Cortical spreading depression triggers migraine attack: Pro," Headache: The Journal of Head and Face Pain **50**, 725–730 (2010), ISSN 1526-4610.

[8] K. Eikermann-Haerter and C. Ayata, "Cortical spreading depression and migraine," Curr. Neurol. Neurosci. Rep. **10**, 167–173 (2010).

[9] S. Akerman, P. R. Holland, and P. J. Goadsby, "Diencephalic and brainstem mechanisms in migraine," Nat. Rev. Neurosci. **12**, 570–584 (2011).

[10] K. F. Bonhoeffer, "Modelle der Nervenerregung," Naturwissenschaften **40**, 301–311 (1953).

[11] R. FitzHugh, "Mathematical models of excitation and propagation in nerve," in *Biological Engineering*, edited by H. P. Schwan (McGraw-Hill, New York, 1969) pp. 1–85.

[12] J. Rinzel and G. B. Ermentrout, "Analysis of neural excitability and oscillations," in *Methods in neuronal modeling*, edited by C. Koch and I. Segev (MIT Press, Cambridge, MA, 1989) pp. 251–291.

[13] E M Izhikevich, "Neural excitability, spiking, and bursting," Int. J. Bifurc. Chaos **10**, 1171–1266 (2000).

[14] J. P. Keener and J. Sneyd, *Mathematical physiology* (Springer, New York, Berlin, 1998).

[15] *Chemical Waves and Patterns*, edited by Raymond Kapral and K. Showalter (Kluwer, Dordrecht, 1995).

[16] E. Schöll, *Nonequilibrium Phase Transitions in Semiconductors* (Springer, Berlin, 1987).

[17] T. Ohta, M. Mimura, and R. Kobayashi, "Higher-dimensional localized patterns in excitable media," Physica D **34**, 115–144 (1989).

[18] K. Krischer and A. S. Mikhailov, "Bifurcation to traveling spots in reaction-diffusion systems," Phys. Rev. Lett. **73**, 3165–3168 (1994).

[19] C. P. Schenk, M. Or-Guil, M. Bode, and H. G. Purwins, "Interacting pulses in three-component reaction-diffusion systems on two-dimensional domains," Phys. Rev. Lett. **78**, 3781 (1997).

[20] Tatsunari Sakurai, Eugene Mihaliuk, Florin Chirila, and K. Showalter, "Design and control of wave propagation patterns in excitable media," Science **296**, 2009–2012 (2002).

[21] Paul C. Bressloff, "Spatiotemporal dynamics of continuum neural fields," J. Phys. A **45**, 033001 (2012).

[22] Y. Lu, Y. Sato, and S. Amari, "Traveling bumps and their collisions in a two-dimensional neural field," Neural. Comput. **23**, 1248–1260 (2011).

[23] P. Bressloff and Z. Kilpatrick, "Two-dimensional bumps in piecewise smooth neural fields with synaptic depression," SIAM J. Appl. Math. **71**, 379–408 (2011).

[24] Z. P. Kilpatrick and G. Bard Ermentrout, "Wandering bumps in stochastic neural fields," SIAM J. Appl. Dyn. Syst. (in press)(2013).

[25] M. A. Dahlem and S. C. Müller, "Migraine aura dynamics after reverse retinotopic mapping of weak excitation waves in the primary visual cortex," Biol. Cybern. **88**, 419–424 (2003).

[26] M. A. Dahlem, F. M. Schneider, and E. Schöll, "Efficient control of transient wave forms to prevent spreading depolarizations," J. Theo. Biol. **251**, 202–209 (2008).

[27] M. A. Dahlem, R. Graf, A. J. Strong, J. P. Dreier, Y. A. Dahlem, M. Sieber, W. Hanke, K. Podoll, and E. Schöll, "Two-dimensional wave patterns of spreading depolarization: retracting, re-entrant, and stationary waves," Physica D **239**, 889–903 (2010).

[28] B. Fioravanti, A. Kasasbeh, R. Edelmayer, D. P. Skinner, J. A. Hartings, R. D. Burklund, M. De Felice, E. D. French, G. O. Dussor, D. W. Dodick, F. Porreca, and T. W. Vanderah, "Evaluation of cutaneous allodynia following induction of cortical spreading depression in freely moving rats," Cephalalgia **31**, 1090–1100 (2011).

[29] D. Levy, M. A. Moskowitz, R. Noseda, and R. Burstein, "Activation of the migraine pain pathway by cortical spreading depression: do we need more evidence?." Cephalalgia **32**, 581–582 (2012).

[30] P. J. Goadsby, R. B. Lipton, and M. D. Ferrari, "Migraine–current understanding and treatment," N. Engl. J. Med. **346**, 257–270 (2002).

[31] J. Olesen, B. Larsen, and M. Lauritzen, "Focal hyperemia followed by spreading oligemia and impaired activation of rCBF in classic migraine," Ann. Neurol. **9**, 344–352 (1981).

[32] B. Grafstein, "Neural release of potassium during spreading depression.." in *Brain Function. Cortical Excitability and Steady Potentials*, edited by M. A. B. Brazier (University of California Press, Berkeley, 1963) pp. 87–124.

[33] G. G. Somjen, "Mechanisms of spreading depression and hypoxic spreading depression-like depolarization," Physiol. Rev. **81**, 1065–1096 (2001).

[34] A. J. Strong, "Dr. Bernice Grafstein's paper on the mechanism of spreading depression," J. Neurophysiol. **94**, 5–7 (2005).

[35] O. Herreras, "Electrical prodromals of spreading depression void Grafstein's potassium hypothesis," J. Neurophysiol. **94**, 3656–3657 (2005).

[36] M. Vincent and N. Hadjikhani, "Migraine aura and related phenomena: beyond scotomata and scintillations," Cephalalgia **27**, 1368–1377 (2007).

[37] A. T. Winfree, "Varieties of spiral wave behaviour: An experimentalist's approach to the theory of excitable media," Chaos **1**, 303–334 (1991).

[38] A. S. Mikhailov and V. S. Zykov, "Kinematical theory of spiral waves in excitable media: comparison with numerical simulations," Physica D **52**, 379–397 (1991).

[39] V. Hakim and A. Karma, "Theory of spiral wave dynamics in weakly excitable media: asymptotic reduction to a kinematic model and applications," Phys. Rev. E **60**, 5073–5105 (1999).

[40] Martin Krupa, B. Sandstede, and Peter Szmolyan, "Fast and Slow Waves in the FitzHugh-Nagumo Equation," J. Diff. Eq. **133**, 49–97 (1997).

[41] H. Kager, W. J. Wadman, and G. G. Somjen, "Simulated seizures and spreading depression in a neuron model incorporating interstitial space and ion concentrations," J. Neurophysiol. **84**, 495–512 (2000).

[42] B. E. Shapiro, "Osmotic forces and gap junctions in spreading depression: a computational model," J. Comput. Neurosci. **10**, 99–120 (2001).

[43] R. M. Miura, H. Huang, and J. J. Wylie, "Cortical spreading depression: An enigma," Eur. Phys. J. Spec. Top. **147**, 287–302 (2007).

[44]R. FitzHugh, "Impulses and physiological states in theoretical models of nerve membrane," Biophys. J. **1**, 445–466 (1961).
[45]J. Nagumo, S. Arimoto, and S. Yoshizawa., "An active pulse transmission line simulating nerve axon.." Proc. IRE **50**, 2061–2070 (1962).
[46]M. Wechselberger, "Existence and bifurcation of canards in $\setminus^3$ in the case of a folded node," SIAM Journal on Applied Dynamical Systems **4**, 101–139 (2005).
[47]G. B. Ermentrout, "Neural networks as spatio-temporal pattern-forming systems," Rep. Prog. Phys. **61**, 353–430 (1998).
[48]A. A. P. Leão and R. S. Morison, "Propagation of cortical spreading depression," J. Neurophysiol. **1**, 33–45 (1945).
[49]Martin Lauritzen, "Cortical spreading depression as a putative migraine mechanism," Trends Neurosci. **10**, 8–13 (1987), ISSN 0166-2236.
[50]R. P. Woods, M. Iacoboni, and J. C. Mazziotta, "Brief report: bilateral spreading cerebral hypoperfusion during spontaneous migraine headache," N. Engl. J. Med. **331**, 1689–1692 (1994).
[51]M. A. Moskowitz, K. Nozaki, and R. P. Kraig, "Neocortical spreading depression provokes the expression of c-fos protein-like immunoreactivity within trigeminal nucleus caudalis via trigeminovascular mechanisms," J. Neurosci. **13**, 1167–1177 (1993).
[52]H. Bolay, U. Reuter, A. K. Dunn, Z. Huang, D. A. Boas, and M. A. Moskowitz, "Intrinsic brain activity triggers trigeminal meningeal afferents in a migraine model," Nat. Med. **8**, 136–142 (2002).
[53]B. K. Ingvardsen, H. Laursen, U. B. Olsen, and A. J. Hansen, "Possible mechanism of c-fos expression in trigeminal nucleus caudalis following cortical spreading depression," Pain **72**, 407–415 (1997).
[54]M. A. Moskowitz and R. Kraig, "Comment on Ingvardsen et al., PAIN, 72 (1997) 407-415," Pain **76**, 265–267 (1998).
[55]X. Zhang, D. Levy, R. Noseda, V. Kainz, M. Jakubowski, and R. Burstein, "Activation of meningeal nociceptors by cortical spreading depression: implications for migraine with aura," J. Neurosci. **30**, 8807–8814 (2010).
[56]P. C. Tfelt-Hansen, "Permeability of dura mater: a possible link between cortical spreading depression and migraine pain? A comment," J. Headache Pain **12**, 3–4 (2011).
[57]B. K. Rasmussen and J. Olesen, "Migraine with aura and migraine without aura: an epidemiological study," Cephalalgia **12**, 221–228 (1992).
[58]F. Wilkinson, "Auras and other hallucinations: windows on the visual brain," Prog. Brain Res. **144**, 305–320 (2004).
[59]R. B. Lipton, D. W. Dodick, S. D. Silberstein, J. R. Saper, S. K. Aurora, S. H. Pearlman, R. E. Fischell, P. L. Ruppel, and P. J. Goadsby, "Single-pulse transcranial magnetic stimulation for acute treatment of migraine with aura: a randomised, double-blind, parallel-group, sham-controlled trial," Lancet. Neurol. **9**, 373–380 (2010).
[60]Benjamin Lindner, J. García-Ojalvo, A. Neiman, and Lutz Schimansky-Geier, "Effects of noise in excitable systems," Phys. Rep. **392**, 321–424 (2004).
[61]S. H. Strogatz, *Nonlinear Dynamics and Chaos* (Westview Press, Cambridge, MA, 1994).
[62]S. D. Silberstein, D. W. Dodick, J. Saper, B. Huh, K. V. Slavin, A. Sharan, K. Reed, S. Narouze, A. Mogilner, J. Goldstein, T. Trentman, J. Vaisma, J. Ordia, P. Weber, T. Deer, R. Levy, R. L. Diaz, S. N. Washburn, and N. Mekhail, "Safety and efficacy of peripheral nerve stimulation of the occipital nerves for the management of chronic migraine: Results from a randomized, multicenter, double-blinded, controlled study," Cephalalgia(2012).
[63]H. C. Diener, "Occipital nerve stimulation for chronic migraine: Already advised?." Cephalalgia(2012).
[64]G. Baier, M. Goodfellow, P. N. Taylor, Y. Wang, and D. J. Garry, "The importance of modeling epileptic seizure dynamics as spatio-temporal patterns," Front Physiol **3**, 281 (2012).
[65]S. J. Schiff, "Towards model-based control of Parkinson's disease," Philos Transact A Math Phys Eng Sci **368**, 2269–2308 (2010).
[66]E M Izhikevich and R. A. FitzHugh, "FitzHugh-Nagumo model," Scholarpedia **1**, 1349 (2006).
[67]R. V. Craster and R. Sassi, "Spectral algorithms for reaction-diffusion equations," Technical Report **99** (2006).
[68]A. S. Mikhailov, *Foundations of Synergetics Vol. I* (Springer, Berlin, 1990).
[69]M. A. Dahlem, F. M. Schneider, and E. Schöll, "Failure of feedback as a putative common mechanism of spreading depolarizations in migraine and stroke," Chaos **18**, 026110 (2008).
[70]A. S. Rojer and E. L. Schwartz, "Cat and monkey cortical columnar patterns modeled by bandpass-filtered 2D white noise," Biol. Cybern. **62**, 381–391 (1990).
[71]T. Bonhoeffer and A. Grinvald, "Iso-orientation domains in cat visual cortex are arranged in pinwheel-like patterns," Nature **353**, 429–431 (1991).
[72]U. Eysel, "Turning a corner in vision research," Nature **399**, 643–644 (1999).
[73]A. Das and C. D. Gilbert, "Topography of contextual modulations mediated by short-range interactions in primary visual cortex," Nature **399**, 655–661 (1999).
[74]C. D. Gilbert, "Horizontal integration and cortical dynamics," Neuron **9**, 1–13 (1992).
[75]C. D. Gilbert, A. Das, M. Ito, M. Kapadia, and G. Westheimer, "Spatial integration and cortical dynamics," Proc. Natl. Acad. Sci. U.S.A. **93**, 615–622 (1996).
[76]E. Niebur and F. Wörgötter, "Design principles of columnar organization in visual cortex," Neural Comp. **6**, 602–613 (1994).